Journal of Energy Storage 31 (2020) 101673

Contents lists available at ScienceDirect

Journal of Energy Storage

journal homepage: www.elsevier.com/locate/est

Hybrid photovoltaic/small-hydropower microgrid in smart distribution network with grid isolated electric vehicle charging system.

Oladepo Olatunde[a,b], Mohammad Yusri Hassan[a,*], Md Pauzi Abdullah[a], Hasimah Abdul Rahman[a]

[a] Centre of Electrical Energy Systems (CEES), Institute of Future Energy (IFE), School of Electrical Engineering, Faculty of Engineering, Universiti Teknologi Malaysia (UTM), 81310 Johor Bahru, Malaysia

[b] Electrical and Electronic Engineering Department, Osun State University, Osogbo PMB 4494, Osun State, Nigeria

ARTICLE INFO

Keywords:
Multi-agent system
Solar photovoltaic
Small hydropower
Electric vehicle
Energy storage system
Smart distribution system

ABSTRACT

The increasing integration of renewable generation and power system innovations toward smartness have made microgrid a platform through which sources of energy could be annexed for efficient network operation. However, the sources must be carefully selected for a synergy to minimize intermittent challenges for productive output. This paper presents a grid-connected load-following hybrid solar photovoltaic and small-hydro microgrid with a grid isolated electric vehicle charging system. A decentralized multi-agent smart voltage network reactive power compensation dynamically regulates and monitors the network limits based on nodes' local measurements. The solar system supports hydropower during the peak load demand and solar storage is charged up by hydropower when irradiation is at the lowest threshold. The energy balance during excess production is configured for individual electric vehicle charging as load points. The photovoltaic-hydropower/electric vehicle microgrid is incorporated with maximum power point tracking and excitation control respectively as a means of control. The detail performance analysis using a time series evaluation over a 24 h daily simulation period is done on standard IEEE 33 and 118-bus radial distribution networks. Consequently, improved voltage regulation, dynamic energy reserve for electric vehicle' charging and a better reduction in power loss are ensured in the research work.

1. Introduction

The global increase in electrical power demand, the impact of environmental pollution and depletion in fossil fuel levels necessitate the need for alternative power sources. The paradigm shift to usage of renewable energy sources (RESs) on distribution system (DS) is more pronounced and will continue in that trend in the nearest future [1]. Distributed energy resources (DER) are integrated into DSs to improve voltage profiles, power quality and system performance [2]. Consequently, the conventional DSs are migrating into multiple interconnected networks embedded with smart applications such as photovoltaic (PV), small hydro plant (SHP) and energy storage systems (ESS) [3]. The agglomeration of different but complementary energy generation systems based on RESs or mixed energy is known as a renewable energy hybrid system [4,5]. Therefore, the resulting grid from this system is known as a microgrid (MG) due to its capacity compared to the main grid.

PV generation is promising and widely exploited all over the world, but the key challenge lies in continuous energy supply. It is weather dependent and impacts technical problems such as power fluctuation and instability [6]. Various approaches, such as demand-side response, a day ahead programming, usage of ESS as a power back up and complementary combination with other RESs are instrumental in alleviating its intermittent challenge. The maximum power point tracking (MPPT) approach is widely used for regulated output, but some of the techniques have a limited operation due to slow tracking and reduced efficiency [7]. Perturbation and observation (P&O) and incremental conductance (INC) methods are common methods by the researchers. However, the operating point in the P&O method results in energy loss due to its oscillation around the maximum power point (MPP). It is not also suitable for frequently changing scenario [8]. The INC offers a better output under a rapidly changing weather with lower oscillation around MPP. It is usually proposed for adaptive variation in voltage step base on the PV curve [9].

The SHP is power distribution compatible, and it is versatile in achieving network balance between voltage profile and reactive power using an excitation system [10]. Hence it is instrumental in providing dynamic support in the smart distribution network (DN). It can

* Corresponding author.
E-mail address: yusrihutm@gmail.com (M.Y. Hassan).

https://doi.org/10.1016/j.est.2020.101673
Received 8 April 2020; Received in revised form 4 July 2020; Accepted 10 July 2020

Nomenclature abbreviation

DSDistribution system Q Distribution system QReactive power
RESsRenewable energy sources V_{AC} Renewable energy sources V_{AC}Alternating current voltage
DERDistributed energy resources V_{DC} Distributed energy resources V_{DC}Direct current voltage
PVPhotovoltaic P_{AC} Photovoltaic P_{AC}Alternating current power
MEGMicro energy grid Q_{com} Micro energy grid Q_{com}Compensating reactive power
SHPSmall hydropower PF_{Δ} Small hydropower PF_{Δ}Change in reactive power
ESSEnergy storage system K Energy storage system KBoltzmann's constant
MGMicrogrid I_{PH} Microgrid I_{PH}Photocurrent
MPPTMaximum power point technique ρ Maximum power point technique ρDiode ideality factor
PVSHPPhotovoltaic small hydropower q Photovoltaic small hydropower qElectron charge
EVElectric vehicle Electric vehicle Voltage angle
PEVPlug-in electric vehicle *Vref* Plug-in electric vehicle *Vref*Reference voltage magnitude
DODDepth of discharge Q Depth of discharge QFlow rate (m^3s^{-1}),
CSVComma-separated values H Comma-separated values HEffective head (m),
MASMulti-agent system η Multi-agent system ηEfficiency
Parameters/variables ρ Water density (kgm^{-3})
ICurrent gCurrent gGravitational constant (ms^{-2}).
ZImpedance T_E Impedance T_EVoltage controller time constant
RResistance ΔV Resistance ΔVVoltage deviation
XReactance T_B Reactance T_BTime constant
YAdmittance K_B Admittance K_BVoltage controller gain
VVoltage T_C Voltage T_CCurrent controller time constant
PReal power E_{fd} Real power E_{fd}Field voltage

replicate the stability and high inertial associated with a centralized hydro generator using a synchronous machine configuration. It possessed excellent efficiency and capacity factor with a reduced rate of fluctuation compare to the wind and solar [11,12]. Ioannis et al. [13] established the degree of complementary between SHP and solar PV by analyzing the hydrological and solar irradiation of a particular case area using an optimization algorithm. The results indicated a significant complementary between the two sources. It was corroborated in [14] and suggested how complementary features can be employed to design hybrid PVSHP for improved efficiency. In general, the combination of compatible and complementary RESs in a microgrid configuration presents a significant potential in a modernized smart distribution network.

Electric vehicle (EV) plays an integral part in modern DNs; the need for a reduction in dependence on fossil fuel and strategic steps to achieve a low-carbon emission transportation system has metamorphosed into the inclusion of EV in DSs [15]. The DNs are generally characterized by a period of deficit generation (peak time) and excess generation (off-peak time). However, one of the strategies to balance up the system at an off-peak time is the inclusion of EV as controllable loads [16]. The DNs are challenged when a plug-in electric vehicle (PEV) is charged in an uncoordinated manner or at peak time. In order to solve this challenge, [17] proposed dedicated charging points through the development of local microgrid. A fast-charging approach was presented in [18] using an AC/DC converter. However, it is a standalone experimental work; its non-coordination with DNs made it challenging to evaluate its performance in active distribution networks (ADNs). Energy management in real-time charging was proposed in [19] for a utility connected plug-in hybrid electric vehicle (PHEV) charging system. The network is managed in the presence of a PV system, and a statistical/probabilistic model was developed to capture renewable uncertainties. However, to successfully incorporate PEV on DNs when RESs are involved, efforts need to be made to cater for downtime or inconsistency in renewable output.

Some researchers devoted attention to the hybridization of PV and wind power, leaving a gap in the complementary combination of PV and SHP [20]. At the same time, some presented a coordinated voltage control with a hybrid microgrid in DSs [21–23]. However, the energy balancing strategy during the excess power production and power deficit in grid-connected microgrid configuration is of paramount significance in the regulated voltage profile. The significant contributions are:

i A grid-connected load following complementary hybrid PV/SHP network injection strategy annexing the MPPT and excitation system as a local means of control
ii Smart distribution coordination through a decentralized multi-agent system interfacing a network power support from micro energy grid integration
iii Unidirectional grid-isolated individual plug-in electric charging/storage system

2. Microgrid architecture

Establishing a complementary synergy between RESs, the PVSHP is hybridized in conjunction with ESS as the energy reserve, as shown in

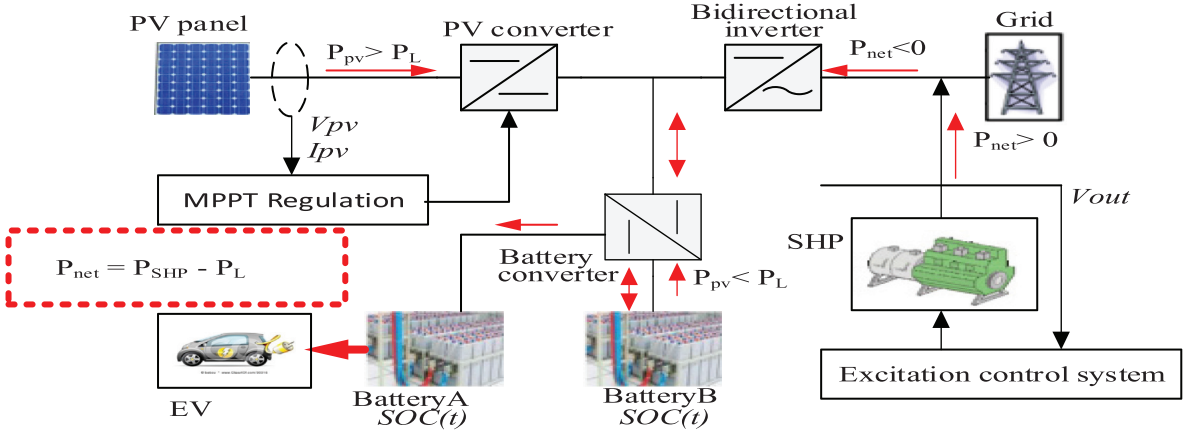

Fig. 1. The proposed grid-connected PVSHP, ESS and PEV in grid isolated mode.

Fig. 1. The MEG is modeled in such that at peak loading conditions, the PV power complements the SHP. Conversely, during the off-peak state, the SHP excess power generation is stored in the battery. The overall excess production is channel toward the electric vehicle charging system as a controllable load. The distribution network is challenged towards voltage collapse when PEV is charged at the peak load of the system. The DN is then stressed and strained beyond the stability limit. In resolving the challenge, the storage for the charging system is configured in grid isolated mode. It can only receive and store power during the excess power generation through a unidirectional converter. In Fig. 1, battery A is designated for the PEV. Battery B provides the energy reserve and power back up for the microgrid and capable of operating in bidirectional mode. The PV and SHP adaptively respond to the network dynamism based on their local measurement with incorporated local means of control. The solar PV is tracked through the MPPT approach, while the excitation system is employed to keep the output voltage of SHP stable despite varying load current at the point of connection. The microgrid is accessed on single and multiple nodes on standard IEEE network over a multi-period daily power flow simulation to evaluate power quality such as voltage profile, power losses and energy gained.

3. PVSHP grid isolated PEV model and control technique

3.1. PV model

The photovoltaic cells are made up of photo-semiconductor devices that can convert solar irradiation directly to electrical energy. It is connected in series and parallel configuration to form an array of PV panels that can generate required direct current (DC) voltage and current output. It is interfaced with a voltage source inverter to produce alternating current (AC) power that is compatible with the distribution power system. A single cell characteristic equation is expressed as [4] and modeled as shown in Fig. 2.

$$I = I_{PH} - I_S\left[\exp\left(\frac{q}{kT_C\rho}(V + RI)\right) - 1\right] - \frac{V + R_S I}{R_P} \quad (1)$$

where I_{PH} is the photocurrent as a function of solar radiation and cell temperature, T_C is the cell's operating temperature, I_S is diode saturation current, K stands for Boltzmann's constant, ρ is an ideality factor of the diode, q is the electron charge, R_P and R_S are the series and parallel resistance of PV cell. The I-V and P-V characteristics of the solar cell as a result of variation in hourly irradiation from 0 to 1000w/m^2 [24–26] using a characterized Kyocera 200Watt grid connect photovoltaic cell is shown in Fig. 4(a) and (b).

3.2. Maximum power point technique

Low generating efficiency of the solar cell is captured by the MPPT to guarantee a maximum power delivery [27]. The incremental conductance (IC) method is adopted in the study because it offers good results under rapidly changing weather conditions. It also has a lower oscillation around the maximum power point, thereby preventing energy loss [9]. It is obtained by differentiating PV power with respect to voltage and equate the result to zero.

$$\frac{dP_{PV}}{dV_{PV}} = I_{PV}\frac{dV_{PV}}{dV_{PV}} + V_{PV}\frac{dI_{PV}}{dV_{PV}} = I_{PV} + V_{PV}\frac{dI_{PV}}{dV_{PV}} = 0 \quad (2)$$

Fig. 3 shows the flow chart for the IC technique. The tracking begins with the PV module's current and voltage within the two instants of time t_1 and t_2. The disparity in voltage and current measured is denoted as dV_{PV} and dI_{PV}, the voltage of the module is then boosted by the duty cycle (C) of the converter until the instantaneous conductance is equal to incremental conductance.

3.3. PV generator capacity

The output of the photovoltaic cells should be able to share in the network load demand when in grid-connected mode with the addition of an extra amount of power due to system losses. The number of PV modules per parallel string in series connection and the number of strings connected in parallel is computed as:

$$N_{\text{modules}/string} = \frac{V_{DCbus}}{V_M} \quad (3)$$

Where $N_{\text{modules}/string}$ denotes the number of the module in a string, $V_{DCbus}$is the direct current bus voltage and $V_M$is the individual module's voltage. A preselected PV panel model for modules configuration and arrangement is employed, as shown in Fig. 5. The amount of parallel string is determined iteratively to meet the required PV output. The hourly generated output power profile of the PV generator based on a different level of irradiation is shown in Fig. 6. The solar irradiance between the first to a fifth hour and twentieth to last hour is zero, hence there is no power output for the period.

3.4. Battery storage capacity

In order to calculate the battery supporting capacity, the maximum current flow at the point of injection is determined by the power flow equation as [28]:

$$P_i = V_i\sum_{j=1}^{N} V_j[G_{ij}\cos(\delta_i - \delta_j) + B_{ij}\sin(\delta_i - \delta_j)] \qquad i \in N \quad (4)$$

$$Q_i = V_i\sum_{j=1}^{N} V_j[G_{ij}\cos(\delta_i - \delta_j) + B_{ij}\sin(\delta_i - \delta_j)] \qquad i \in N \quad (5)$$

$$I_i = \sum_{j=1}^{N} y_{ij}(V_i - V_j) \qquad i \in N \quad (6)$$

Where $Y_{ij} = G_{ij} + jB_{ij}$ is the system admittance matrix, P_i and Q_i are the real and reactive power injected at bus i respectively. The battery current is determined by as [29]

$$I_{bat}(t) = \frac{V_{AC}(t)*I_{AC}(t)*\cos\theta}{V_{DC}(t)*\eta_{inv}} + I_{DC}(t) = \frac{P_{AC}}{V_{DC}(t)*\eta_{inv}} + I_{DC}(t) \quad (7)$$

Where $V_{AC}$is the ac voltage, V_{DC} is dc voltage, cos θ is ac load power

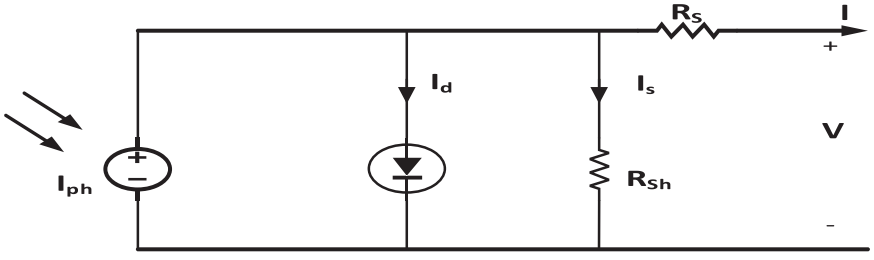

Fig. 2. One diode model of photovoltaic cell.

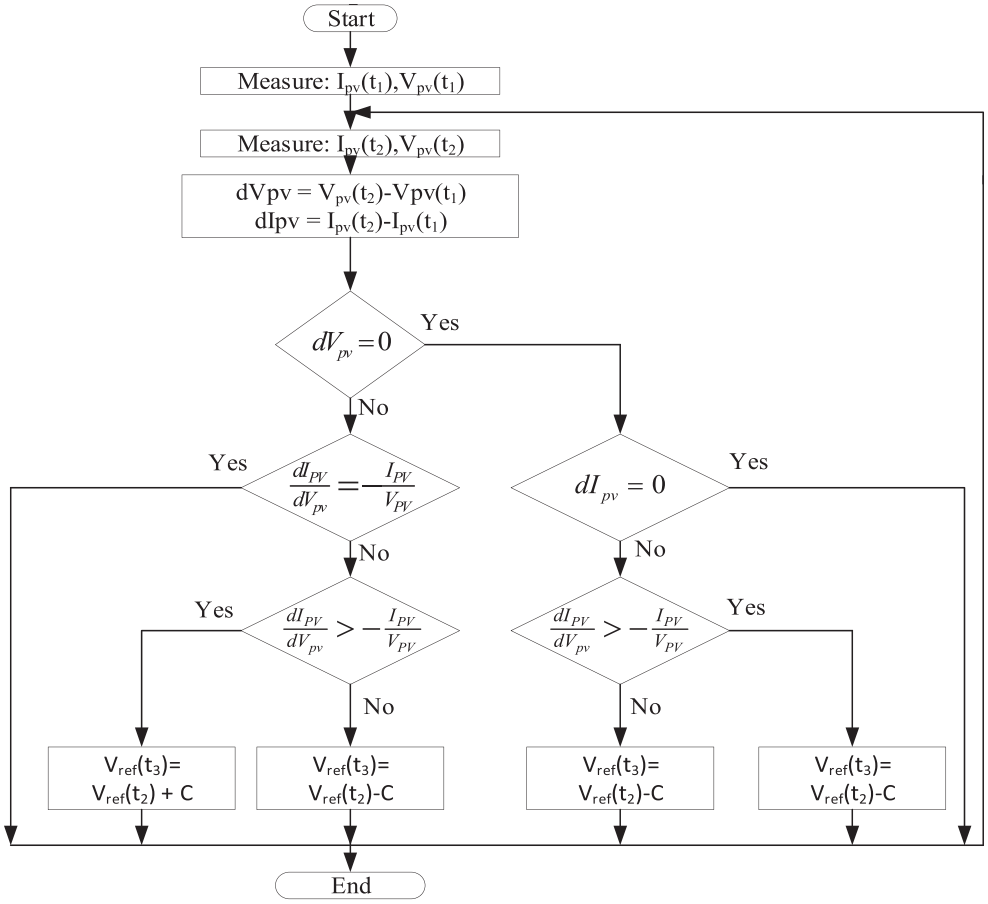

Fig. 3. IC technique.

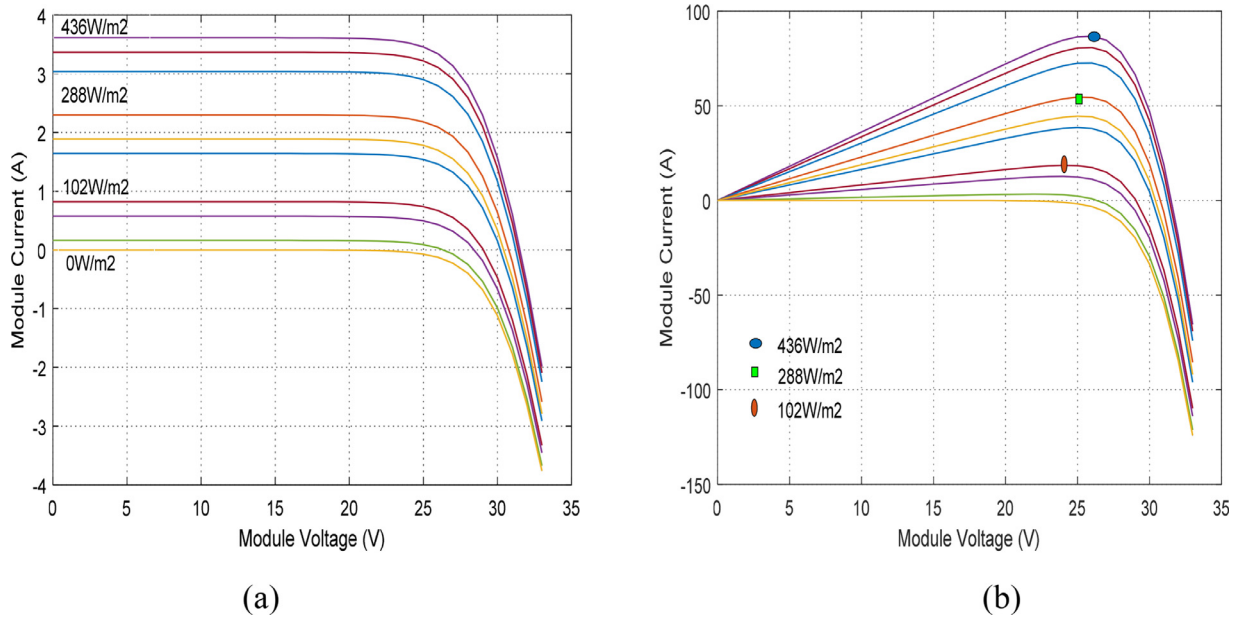

Fig. 4. (a). *I-V* curves for hourly irradiation levels (0–436W/m^2 at 25°C) (b) *P-V* curves for hourly irradiation levels (0–436W/m^2 at 25°C).

factor and η_{inv} is the inverter efficiency. The power output profile of the inverter is shown in Fig. 7 using the efficiency of 0.95. The battery charges when the network applied voltage is higher than the battery voltage and discharges when the battery voltage is more significant than the network voltage. Based on the calculated maximum current flow at each point of power injection, 500Ah individual battery capacity is combined in a series-parallel connection to achieve the system storage capacity for each of the microgrids integrated. The battery state of charge (SOC) is determined using [29]:

$$I_{bat\_Ah}(t) = I_{bat\_Ah}(t-1) + (-I_{load}(t)) \quad (8)$$

The arrangement of the grid-tied preselected battery is shown in

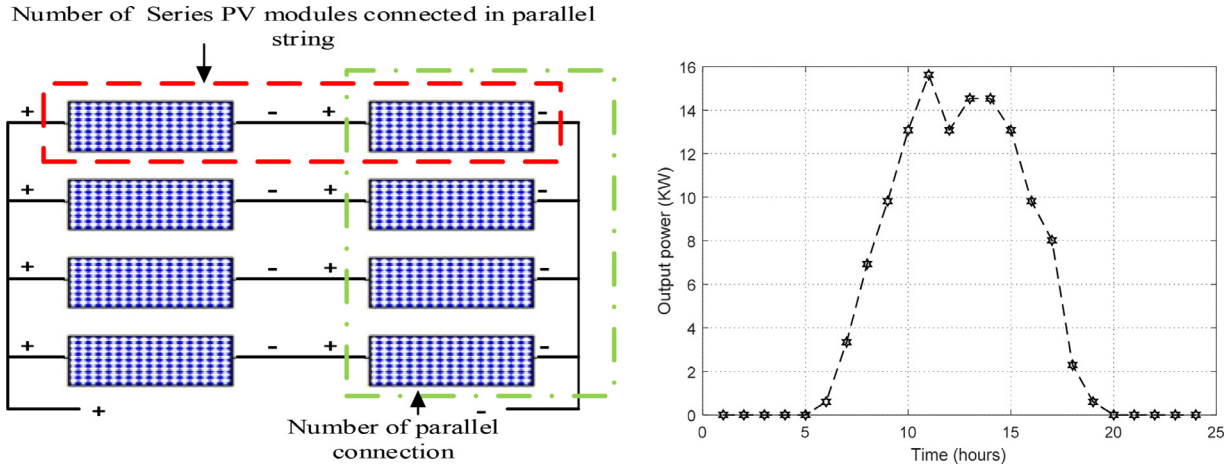

Fig. 5. Series and parallel connection of PV modules.

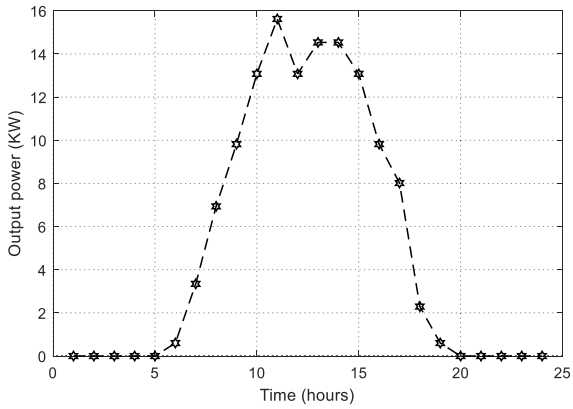

Fig. 6. The hourly output power profile of the photovoltaic generator.

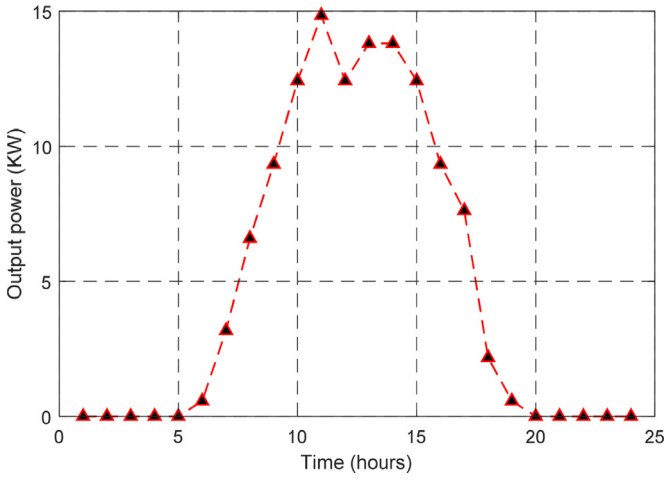

Fig. 7. The hourly power output of the inverter.

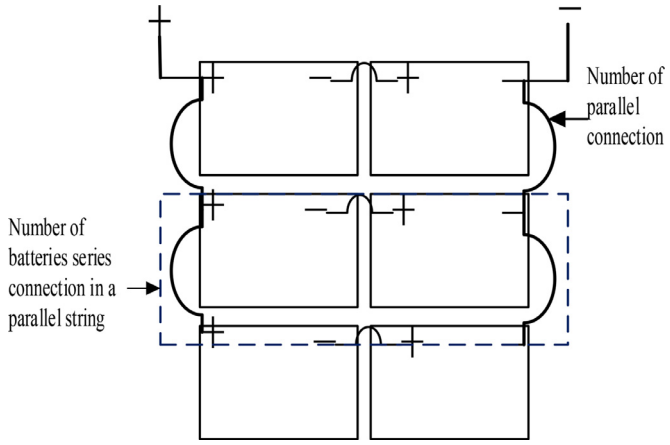

Fig. 8. Battery arrangement and configuration.

Fig. 8, the series connection of the battery to form the parallel strings is determined as [29]:

$$N_{bat\_series} = \frac{V_{DCbus}}{V_{bat}} \tag{9}$$

Where N_{bat_series} denotes the number of battery in series connection, V_{bat} is the individual battery voltage and V_{DCbus} is the voltage at the direct current bus. The battery output capacity is determined by:

$$P_{total\_bat\_output} = P_{total\_bat} * 2(50\%DOD) * 0.95 \tag{10}$$

Where P_{total_bat} denotes the total battery power, DOD is the depth of charge which is the minimum lowest threshold the battery can discharge. It is usually incorporated to prolong the service years of the battery and 0.95 is the system efficiency.

3.5. Small hydropower

A small hydropower plant has less impact on the environment and ecosystem. Its power production is a function of the flow rate of a stream or dam water discharge. A simple expression of the power output for a small hydro-plant as given by [13]:

$$P = QH\eta\rho g \tag{11}$$

Where P is the output power (W), Q is the flow rate (m^3s^{-1}), H is the effective head (m), η is the efficiency, ρ is the density of water (kgm^{-3}) and g is the gravitational constant (ms^{-2}). SHP has the ability to mimic the stability and high inertia of conventional centralized hydro generator with a reduced rate of fluctuation. The net head is taking to be fairly constant for a particular season of the year adapted for the study. The water flow rate does not reflect significant fluctuation on an hourly basis; therefore, the output of the SHP is assumed to be constant on its daily profile. The SHP potential by countries over the world is shown in Fig. 9, which placed Nigeria on the better potential for power generation in African countries [30]. The flow pattern and characteristics are obtained from the ministry of water resources and rural development, Osun state government of Nigeria [31].

The voltage regulator deviation of SHP at point of connection is mathematically expressed as [32]:

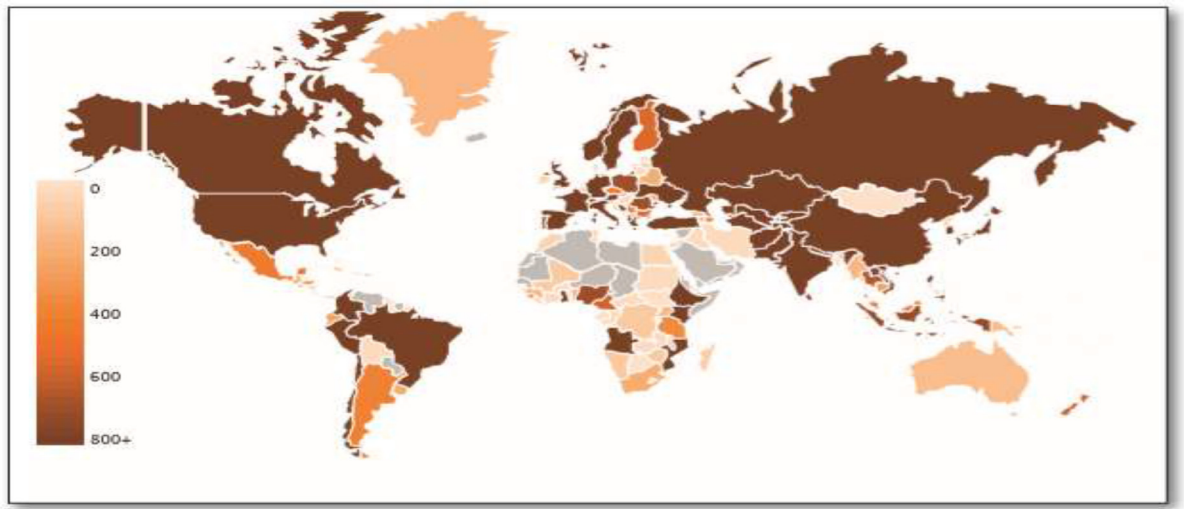

Fig. 9. The SHP potential by countries in the world [30].

$$\Delta V = V_{ref} - V_{pcc} \tag{12}$$

First amplifier stage in voltage controller using first order differential equation in per unit is:

$$\frac{dx_1}{dt} = -\frac{x_1}{T_E} + K_E.\frac{\Delta V}{T_E} \tag{13}$$

Second amplifier stage in voltage controller is evaluated using:

$$\frac{dx_2}{dt} - \frac{x_2}{T_B} + \left(1.0 - \frac{T_A}{T_B}\right).\frac{x_1}{T_B} \tag{14}$$

Current regulator deviation, first and second stage current controller amplifier is evaluated using:

$$\Delta I = I_{fd_{ref}} - I_{fd} + x_2 + T_A.\frac{X_1}{T_B} \tag{15}$$

$$\frac{dx_3}{dt} = -\frac{x_3}{T_1} + AKI.\frac{\Delta_I}{T_I} \tag{16}$$

$$\frac{dx_4}{dt} = -\frac{x_4}{T_D} + \left(1.0 - \frac{T_C}{T_D}\right).\frac{x_3}{T_D} \tag{17}$$

The field voltage is determined using:

$$E_{fd} = E_{fd0} + x_4 + T_C.\frac{x_3}{T_D} \tag{18}$$

The field voltage is proportional to terminal voltage of the generator as:

$$E_{fd} = E_{fd} + \frac{E}{V_{ref}} \tag{19}$$

3.6. Grid isolated electric vehicle charging

The charging system is isolated from the grid through a unidirectional converter, which implies the converter can only feed the battery system designated for electric vehicles. It cannot return power to the network from the battery. The arrangement is to mitigate the technical challenge that has to do with the fact that PEV owners in the same society may share the same social lifestyles. The grid might be subjected to peak demand when PEV owners are back from work at the same time. It also technically avoid the network being thrown into the state of collapse at peak load time with an indiscriminate plugin of EVs. The

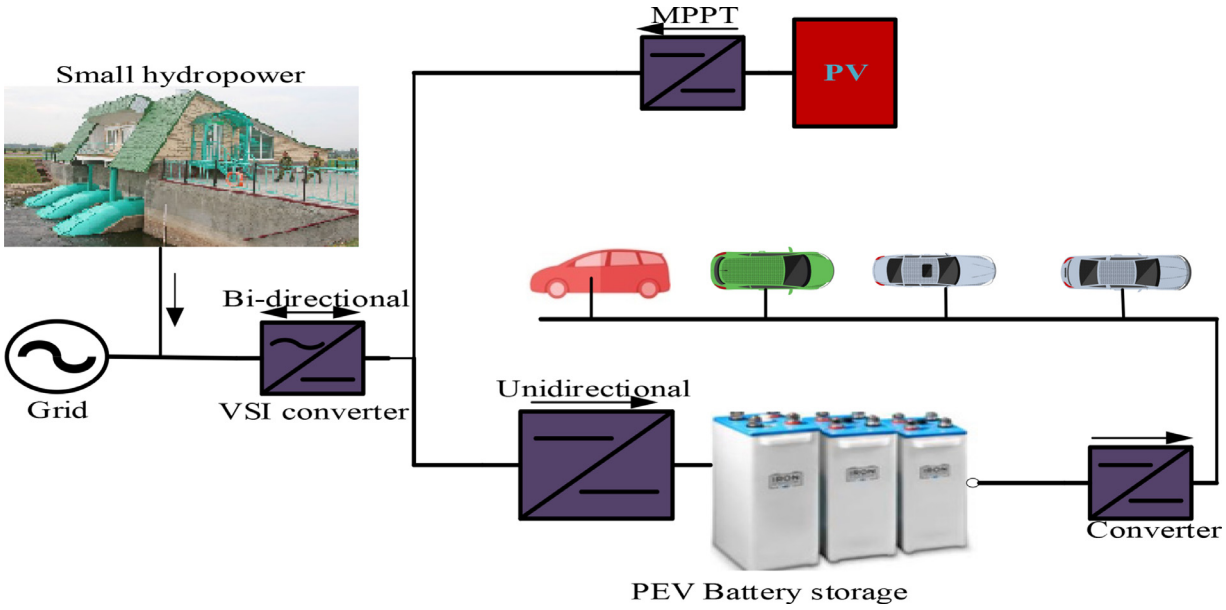

Fig. 10. One-line diagram of grid isolated electric vehicle charging system.

unidirectional converter is an ac-dc voltage source inverter feeding the power storage facility provided for the PEV, as shown in Fig. 10. The power demanded by the PEV can be calculated by [19]

$$P_{PEV} = \frac{M_d \times E_m}{D_t - A_t} \tag{20}$$

Where P_{PEV} is the power demanded by the PEV, E_m is the energy consumption per mile,M_d is the daily number of miles covered, D_t is the departure time after charging, A_t is the arrival time. As a strategy to prolong service years of the vehicle battery, the upper and lower threshold of their SOC is usually enforced. The lower limit is always incorporated in the vehicle while the upper limit is monitored at the charging station. Four classifications of vehicles were considered for the PEV energy storage charging system, as shown in Table 1.

Three cases of charging time are considered: a charging time that commenced by 17.00hour of the day, which assumed the same social lifestyle of the society. It takes into consideration that most vehicle users must have come from various working offices. The second charging time considered a twenty- four hours changing system in which the vehicle users can arrive for charging at any hours of the day. And the last employed a random generation of vehicle class, charging time and consumption/mile using the normal distribution as presented in [33] using Matlab random function.

The summation of power demanded by ith PEV is expressed as:

$$P_{PEVD} = \sum_{i=1}^{n} P_{PEV}(i) \tag{21}$$

Where P_{PEVD} is the summation of power demanded by all P_{PEV} connected, P_{PEV} is the individual electric vehicle connected. The value is discharge in real-time from the energy storage charging system.

4. Proposed methodology and algorithm flowchart

The PVSHP/ESS/EV MEG is grid-connected, but the EV charging system is isolated through a unidirectional converter. The load-following coordination technique is employed, and the MEG responds to reflect the network dynamism. The load-following method is a load current (I_L) based model, in which the instantaneous magnitude of load demand determines the direction of microgrid power dispatch. The power injected by the microgrid and the power reverse from the main grid changes direction alternatively as the magnitude of load demand varies. The source file containing load, meteorological data is prepared in CSV format on the spreadsheet program for multi-period power flow analysis to evaluate the network performance. Standard IEEE 33 bus and 118 bus system specifications are also defined.

The computing process begins by evaluating the current generated by the SHP (I_{SHP}). The SHP stands as the core and leads generating source to the main grid. The I_{SHP} compares the main grid network load current (I_L). The load current is determined by the microgrid compactible backward/forward sweep power flow analysis in real-time simulation model using the branch injection to bus current (BIBC). The current produced by the PV (I_{PV}), the battery state of charge (SOC), the charging current (I_{ch}) and the discharging current (*Idisch*) were all computed and stored in matrices with a different identifier.

The system model operates in three scenarios: the first case becomes operational when SHP generated current is equal to the load current ($Inet = 0$). It implies load is complete fulfillment by the SHP. However, there is no excess energy for battery charging and vehicle storage. In the second case, the SHP supply is more than the load current. There is power demand fulfillment; hence the excess energy charges the battery. At fully charged battery conditions, the excess is diverted to the EV charging storage system. However, if the battery SOC is less than the maximum status, the battery is charged, and the new SOC is computed. The last case occurs when the SHP supply is less than the load current. The battery SOC is checked; if the battery SOC is higher than the minimum SOC (*SOCmin*), the battery supports the SHP in fulfilling the network load demand. However, if the battery SOC is less than the minimum (*SOCmin*), the PV support the system in achieving the network load demand. Fig. 11 shows the flowchart of the proposed PVSHP/ESS/EV MEG load-following technique.

A time-dependent power flow analysis suitable for the microgrid active distribution network is adopted using the backward/forward sweep approach. The network load demand, power supplied by the PV, ESS, and the MEG are dynamically changing over a twenty-four hours simulation to account for variability and network dynamism. The analysis begins from one branch to the other until all the branches on the feeder are traced. Initially, the voltages for all the buses are assumed to take the value of 1 per unit (pu) and zero voltage angle. Using the initial voltage and specified real and reactive power, the branch current is computed from the end bus to the source (Backward Sweep). The branch current is determined to find the voltage drop, the real and reactive power losses in the system. The current at the source bus is then calculated as expressed by [35].

$$I = \sum_{\substack{i=1 \\ i\neq s}}^{n} P_i + \sum_{\substack{j=1 \\ i=1 \\ i=j}}^{n} P_{loss.ij} + \left(\sum_{\substack{i=1 \\ i\neq s}}^{n} Q_i + \sum_{\substack{j=1 \\ i=1 \\ i=j}}^{n} Q_{loss.ij} \right) / V_s^* \tag{21}$$

$$Z_{ij} = R_{ij} + jX_{ij} \tag{22}$$

$$V_{Drop.ij} = V_j - V_i = I_{ij} Z_{ij} \tag{23}$$

$$P_{loss.ij} = I_{ij}^2 R_{ij} \tag{24}$$

$$Q_{loss.ij} = I_{ij}^2 R_{ij} \tag{25}$$

Where:

$\sum_{\substack{i=1 \\ i\neq s}}^{n} P_i$ is the sum of real load connected the receiving end buses; $\sum_{\substack{i=1 \\ i\neq s}}^{n} Q_i$ is the sum of reactive load connected the receiving end buses; $\sum_{\substack{j=1 \\ i=1 \\ i=j}}^{n} P_{loss.ij}$ is the sum of the branch (*ij*) real power loss across the feeder;

$\sum_{\substack{j=1 \\ i=1 \\ i=j}}^{n} Q_{loss.ij}$ is the sum of the branch (*ij*) reactive power loss across the feeder; V_s^* is the conjugate of the source voltage; I is the current at the source end; $Z_{ij}$is the impedance of branch *ij;* R_{ij} is the resistance of branch *ij;* $X_{ij}$is the reactance of branch *ij;* $V_{Drop.ij}$is the voltage drop across the branches *ij;* V_j and V_i are the voltage at bus j and i respectively; I_{ij} is the current flowing through bus *i* to *j*.

The computation then begins at the source bus toward the end node to evaluate the voltage drop using Eq. (23), branch current (I_{ij}), real and reactive power losses using Eqs. (24) and (25) respectively (Forward Sweep). At the completion of the process, the total losses are calculated, and the power mismatched is determined. The process is repeated when the MEG is integrated. The percentage improvement in performance indices is evaluated. Fig. 12(a) shows the proposed load flow methodology used for this study.

The capacitor banks provide network voltage support in terms of reactive power compensation. However, using a decentralized multi-agent system (MAS), the compensating injected reactive power is evaluated by dynamic computation of voltage and power factor

Table 1.
Classification of vehicles [34].

Vehicle class	Description	Consumption/mile
1	Compact passenger cars	0.3kWh/mile
2	Full size passenger cars	0.45kWh/mile
3	Medium-size SUV and pick-up trucks	0.6kWh/mile
4	Large size SUV and pick-up trucks	0.75kWh/mile

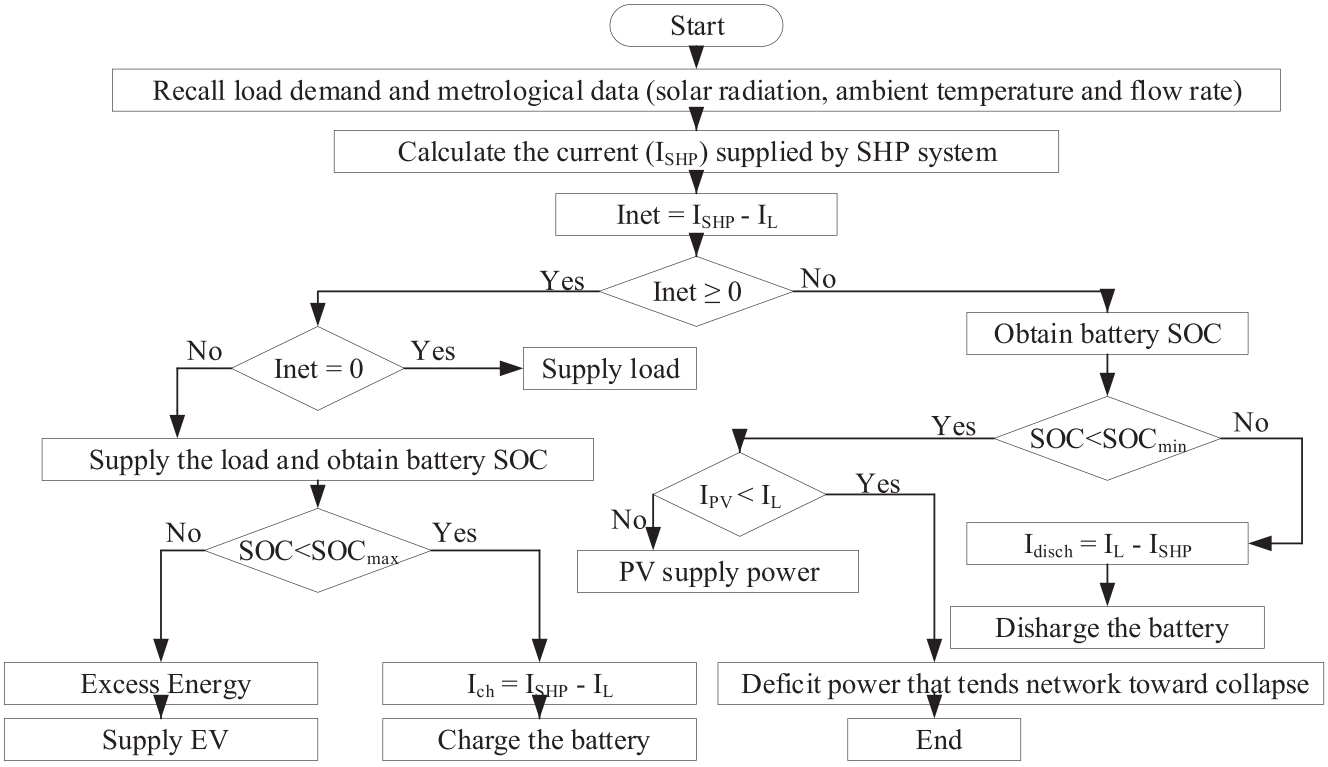

Fig. 11. Load following technique system design flowchart.

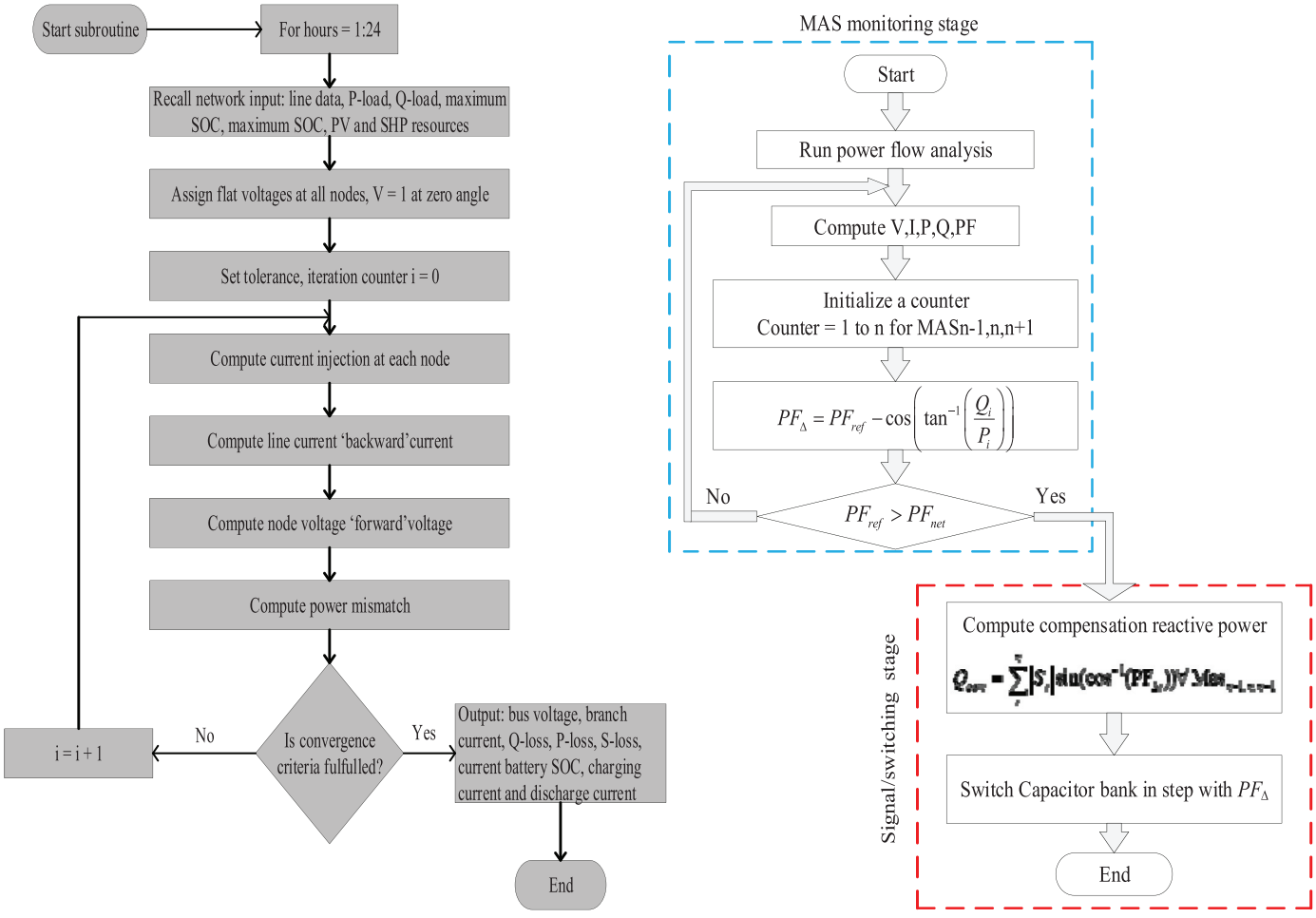

Fig. 12. (a). Proposed load flow methodology. Fig. 12 (b) Proposed network dynamic reactive power injection.

variation on nodes of the feeder. The dynamic computation of network parameters determines the compensating injected reactive power Q_{com} on a real-time basis. The capacity of the dynamically evaluated Q_{com} determines the step switching sequence of the capacitor banks. Fig. 12(b) shows the network operational flowchart for the dynamic MAS coordination of capacitor step switching. However, SHP generates both real and reactive power; therefore the absolute reactive power compensation is also sourced from the microgrid to relieve the stress on CBs.

5. Test system and simulation cases

Simulation of the study models validates the effectiveness of the grid-connected complementary hybrid hydro-photovoltaic MEG load following technique in grid isolated PEV using standard IEEE 33 and 118 bus system. Fig. 13 shows the thirty-three bus system, it contains the main feeder, three laterals and thirty-two branches. The total loads are 3.72 MW and 2.3MVAr. The substation voltage is 12.66kV at the base power of 100MWA [1]. Fig. 14 shows the IEEE 118 bus system with a substation voltage of 11kV. It comprises of a slack bus, 117 branches and load buses [36]. It has a total power load of 22709kW and 17041kVAr [37]. The simulation presents the twenty-four hours multi-period dynamic load changing scenario in which voltage is coordinated at each hour toward the operating statutory bound. Hybridization of small hydropower with photovoltaic power in conjunction with EES therefore forms a reliable micro energy grid. SHP provides energy in both day and night and solar PV serves as back up energy supply during the peak hours of the day. The SHP continues the supply of charging current to the PEV energy storage charging system during the hours when solar irradiation is unavailable. The power demand by various classes of vehicle, number of vehicle and battery SOC are also evaluated in real time and analysed. Results are analyzed based on hybrid PVSHP/ESS MEG smart DN and grid isolated PEV charging system.

5.1. Proposed hybrid PVSHP smart network with grid isolated electric vehicle charging system

In this model, the capacitive reactive power compensation for network voltage regulation is dynamically evaluated at each hour using the decentralized cooperative multi-agent system. The dynamic reactive power compensation works in synergy with MPPT solar PV and SHP exciter control based on the local measurement at the point connection. Fig. 11 shows the microgrid load following approach flowchart. The network and microgrid harmoniously respond to dynamism based on load following technique.

Fig. 15 shows the voltage profile of the proposed model compared to the base, with the integration of one hybrid microgrid. The minimum voltage at the base case is 0.8765 pu at 20.00 hour. The value moved up to 0.9698 pu at the same hour, while the maximum voltage is 1.002 pu with a proposed model. In the scenarios earlier discussed, the voltage profile was unachievable within the statutory limit in all the hours of the day. However, for the proposed model, the voltage operates within the statutory limit at all hours of the day. The percentage voltage improvement achieved is 48% at losses reduction of 39%. Fig. 16(a) shows the online capacitor injection step per hour and Fig. 16(b) shows the power injection by both solar PV and SHP generators. Fig. 17 shows the voltage profile per hour with one hybrid microgrid, operated within the statutory bound.

With the integration of two hybrid microgrids at different nodes along the DN feeder, the minimum voltage of 0.8765 pu at 20.00 hour for the base case improved to 0.9696 pu within the operating bound. The maximum voltage is also 1.038 pu. Fig. 18 shows the voltage profile of the proposed model with two hybrid microgrid injections. The percentage voltage improvement is 72%, while the percentage power loss reduction is 33%. In every hour of the day, the voltage falls within the operating bound, as shown in Fig. 19. Table 2 shows the summary of voltage profile and power losses.

The microgrid ESS backs up and supports the main grid when the SHP cannot meet up the load demand at any hour of the day. It occurs at the hour the load current (I_L) is higher than (I_{SHP}), which implies *Inet* is negative. In Fig. 20(a), the battery injected power into the main grid at 03.00 hwith its SOC discharged from its *SOCmax* 200kA to 179kA. The *Inet* turned positive from 04.00 h; the SHP again takes up power injection, and ESS goes to charging mode. Another battery discharge is again experienced at 20.00 h of the day. The second microgrid (MG2) experienced a constant positive *Inet* with the battery SOC maintained at maximum state at all hours of the day. Fig. 20(b) shows the charging and discharging current of the microgrid battery for the day.

At maximum battery SOC, the excess charging current is diverted for storage in the PEV storage charging system. Starting with minimum initial battery SOC for PEV battery storage (50% SOC of the PEV battery storage capacity), the EV battery charging system and the EVs connection for charging are set on simultaneously. The daily SOC is monitored to ascertain the level of storage at each hour and the number of vehicle types that can be conveniently charged. The procedure is repeated when the initial battery SOC is 80% charged. Fig. 21(a) shows the PEV battery storage SOC for the two microgrids integrated into the main network. The EVs connection for charging considering vehicle class, charging time and miles per day are presented in three cases.

Case A: In this case, the initial battery SOC is at the minimum (100kVA), and the charging time commenced by 17.00 h of the day. It assumed users must have closed in their various offices and be ready for charging. Fig. 21(b) shows the SOC without EV connection in comparison with EVs connected. 30 number of compact passenger vehicle class EVs were connected, and the system signifies low battery at 17.00 to 21.00 h as indicated with the red curve in the plot. When the EVs connection was reduced to 20, the system shows a low battery at 17.00–20.00 h. It implies that the charging system could not

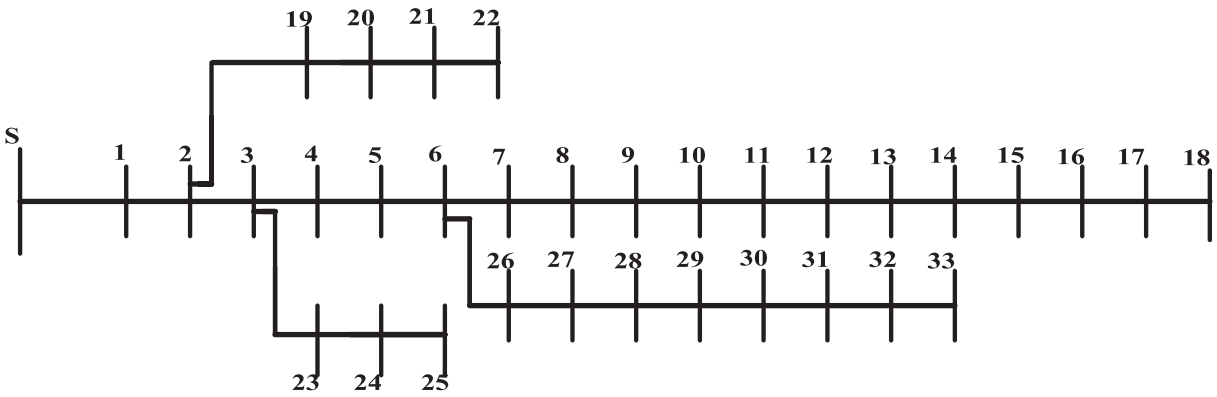

Fig. 13. Single line diagram of 33bus test system [1].

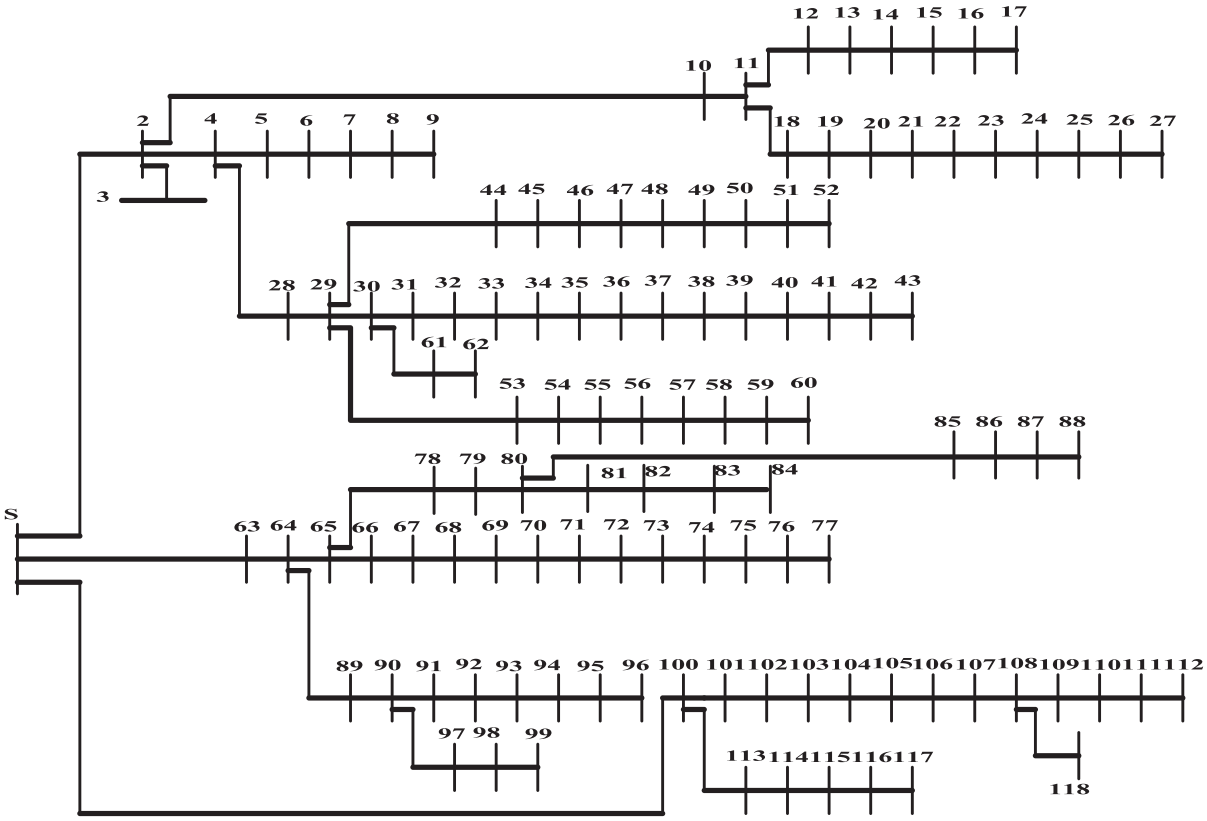

Fig. 14. Single line diagram of 118 bus system [36].

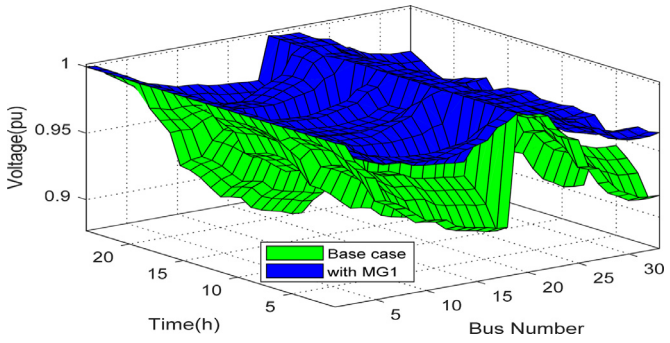

Fig 15. Voltage profile of the proposed model with one hybrid microgrid injection.

accommodate up to 20 EVs connection. However, the PEV changing system could accommodate 19 EVs connection without indication of low battery in any of the hours. Table 3 present the number of EVs accommodation as the charging time, vehicle class and mile per day vary. The red curve in Fig. 22(a) shows that the system signifies a low battery status from 0.00 h to 21.00 h due to overloading with EVs connection.

Case B: In this case, the initial battery SOC is at maximum and the charging time covers the whole 24.00 h of the day. Different charging time, vehicle class and miles per day were selected and combined. The number of EVs connection were evaluated and presented in Table 3.

Case C: In this case, the initial battery status is fully charged, the charging covers the whole hours of the day. However, the vehicle class, the charging time and the miles per day were randomly selected using the metaheuristic particle agents and computed for online evaluation

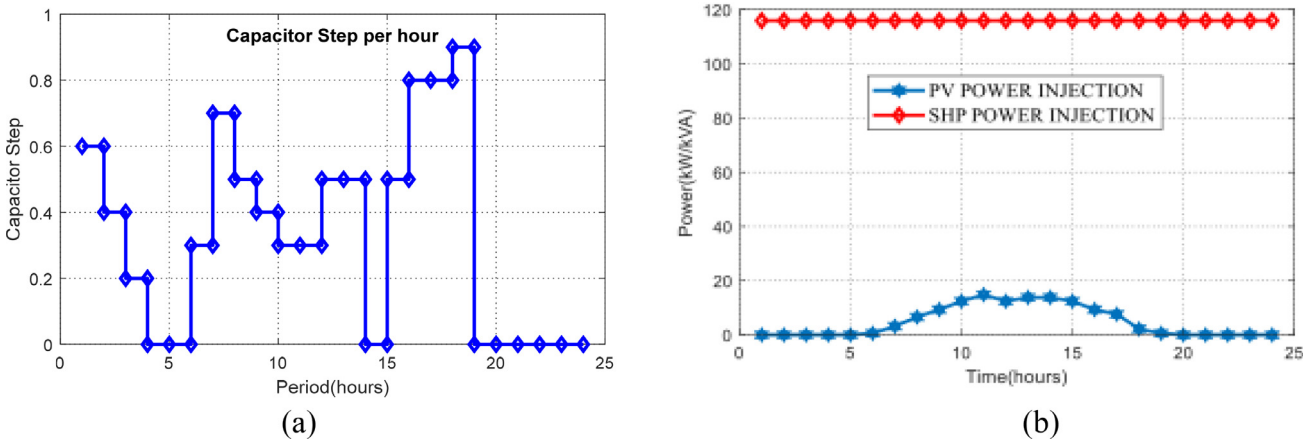

Fig. 16. (a). Capacitor steps for the online reactive power injection (b) Power injection by solar PV and SHP generators.

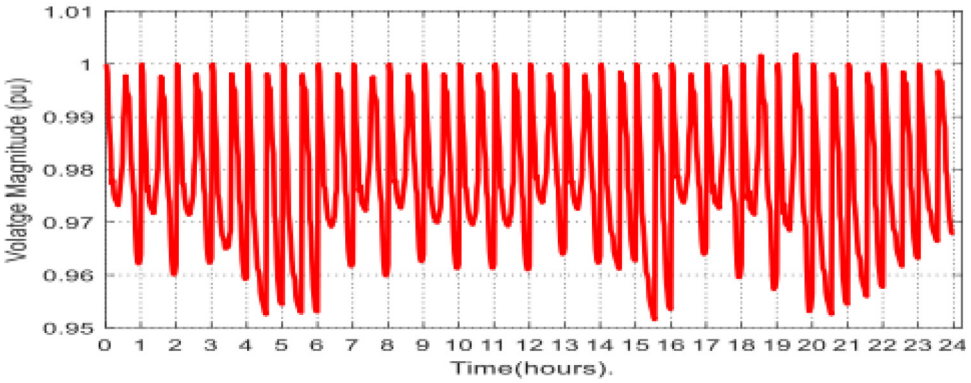

Fig. 17. Voltage profile per hour with one hybrid microgrid with the statutory bound.

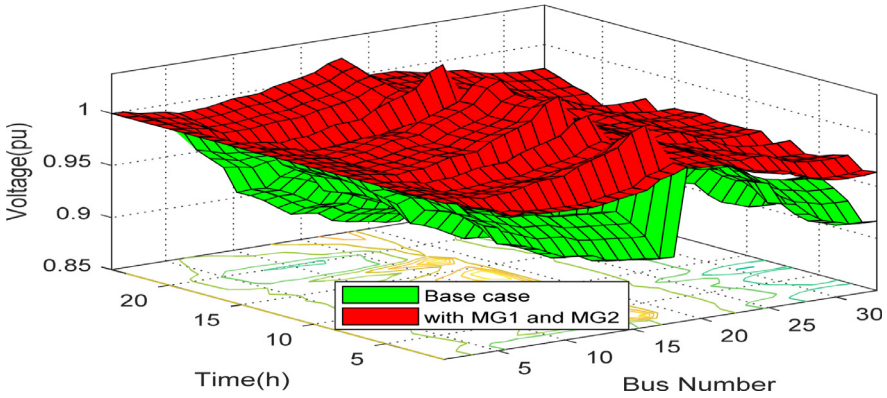

Fig. 18. Voltage profile of the proposed model with two hybrid microgrid injection.

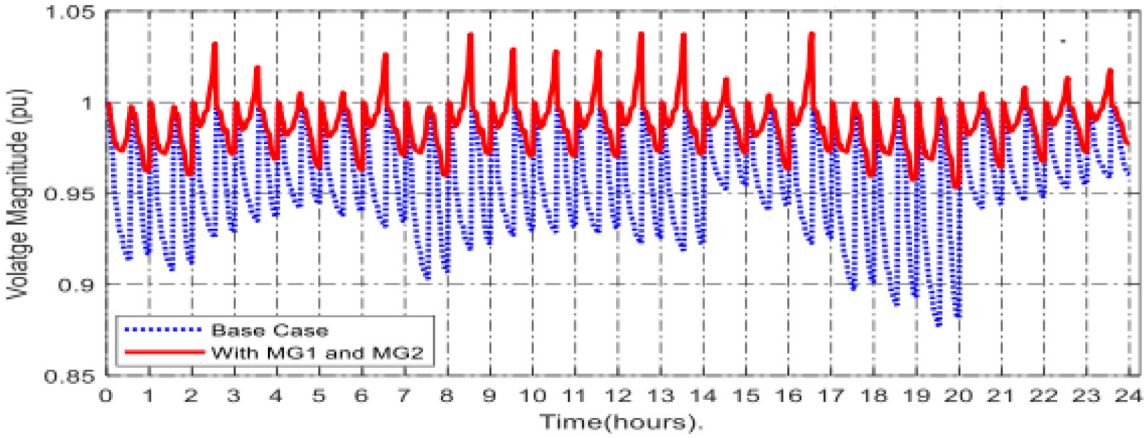

Fig. 19. Voltage profile per hour with two hybrid microgrids with the statutory bound.

Table 2.
Shows the summary of voltage profile and power losses.

Items	Without DG	With DG				With MG(Proposed model)	
		One DG PV @bus 18	SHP @bus 18	Hybrid PVSHP centralizes@ bus 18	PVSHP decentralized @bus 2&18	One MG PVSHP/ESS @ bus 2	Two MG PVSHP/ESS @bus 2&18
Total losses(base)kW	4587	4587	4587	4587	4587	4587	4587
Total losses(kW)		4217	2954	3377	2938	3695	3525
Loss reduction (%)		08.09	35.62	26.38	35.96	39.46	33.17
Min voltage	0.877 @bus 18,20h	0.9699 @bus 18,20h	0.9699 @bus 33,20h	0.9699 @bus 33,20h	0.9699 @bus 33,20h	0.9698 @bus 18,16h	0.9696 @bus 30,20h
Max voltage	1.000 @bus 1&2,	1.017 @bus 18,15h	1.029 @bus 18,20h	1.076 @bus 18,20h	1.029 @bus 18,20h	1.002 @bus 18,20h	1.038 @bus 18,13h
Voltage imp (%)		05.90	30.48	35.47	30.64	48.55	72.39

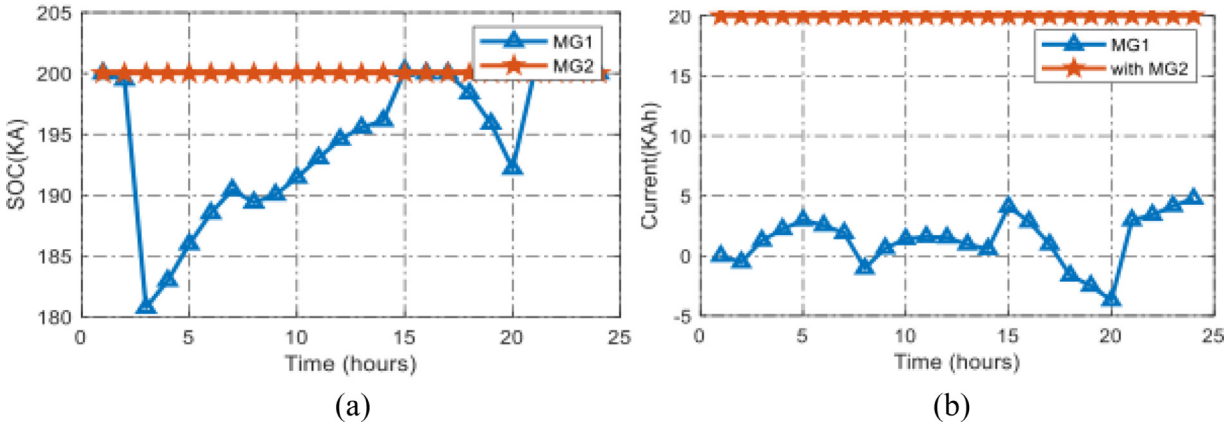

Fig. 20. (a). The battery state of charge for MG1 and MG2 (b) Battery charging and discharging current.

on the system charging system. One hundred particles for vehicle class, charging time and miles per day were randomly combined. Fig. 22(b) show the percentage of each category of vehicle selected. The medium size SUV and pick-up trucks has the highest selection at 31%.

Fig. 23(a) shows the cumulative EVs connection for each combination of particle agents. The medium size SUV and pick-up trucks with the highest percentage of vehicle class have the highest cumulative of 2679 EVs. The selected one hundred vehicle class combination is also evaluated for the number of miles for each combination and the number of EVs that could be connected for charging. Fig. 23(b) shows the number of miles and that EVs connection for charging for each combination of vehicle class. The number of miles per day ranges between 80 miles to 120 miles, while the EVs number ranges between 60 and 120. The vehicle class distribution in one hundred vehicle class combinations is shown in Fig. 24.

IEEE 118-Bus system: the proposed model was also tested on a more extensive network for comparative analysis, the network was analyzed in terms of voltage profile improvement and power loss reduction and results were computed and compared. The voltage profile of the proposed model with the integration of four MEG at bus 2, 33, 77 and 118 is shown in Fig. 25. The nodes were selected through the voltage stability index estimation. The bus with the lowest voltage is at bus 77 with value 0.8665(pu) at 20.00 h. The base case improves to 0.9232(pu) at the integration of MEG. The percentage improvement in voltage profile and reduction in power losses is presented in Table 4. However, the operation of voltage within the statutory bound continues to increase as more MEG is integrated on the network. With the integration of four microgrids along the feeder, the voltage operation with the limit is achieved in all the buses at all hours.

Table 3.
EVs system accommodation at varying charging time, vehicle class and consumption per mile.

Initial SOC – Minimum SOC (Case A)					Initial SOC – Fully charged (Case B)				
Energy/ mile kWh/ mile	PD (kW)	No of mile	Hours	No of EVs	Energy/ mile kWh/ mile	PD(kW)	No of mile	Hours	No of EVs
0.30	0.750	20	8	19	0.30	0.750	60	8	79
0.45	1.125	20	8	12	0.45	1.125	60	8	53
0.60	3.000	20	4	4	0.60	1.500	60	8	39
0.60	1.500	20	8	8	0.60	3.000	60	4	19
0.75	1.875	20	8	7	0.75	1.875	60	8	31
0.75	3.750	20	4	3	0.75	3.750	60	4	15

Fig. 26 shows the voltage profile at bus 77 of the feeder at the integration of different number of microgrids. The highest-profile is observed at the inclusion of four microgrids.

To verify the ability of the proposed model: utility connected complementary hybrid hydro-photovoltaic multi-microgrid in smart distribution network with grid isolated electric vehicle charging system. A comparison is made with three selected existing works [1,38,39]. The renewable energy configuration and method adopted in the works are summarized in Table 5. In this research, a decentralized multi-agents smart operation and regulation of the reactive power support combines the load following complimentary combination of hybrid solar PV and SHP with their built-in MPPT and excitation control. The results reflected a considerable improvement in voltage profile, and with two MGs integration at bus 2 and 18, the voltage successfully operated with

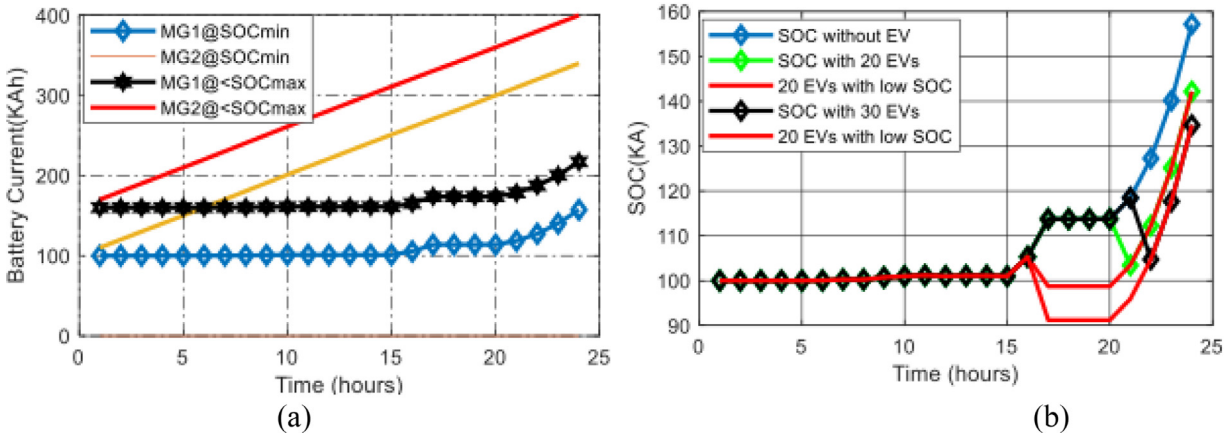

Fig. 21. (a). The PEV battery storage SOC without EVs connection (b) PEV battery storage SOC with EVs connection.

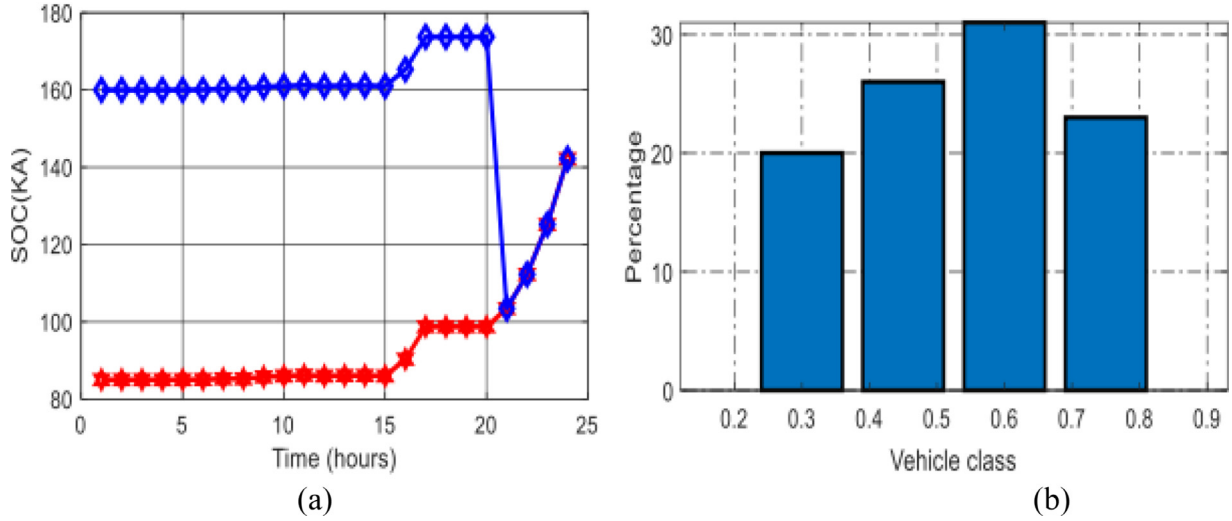

Fig. 22. (a) PEV storage system signifying a low battery status (b) Percentage of vehicle class.

the statutory limit at all feeder nodes, as shown in Fig. 19. However, in the method adopted in [1], the voltage operation within the bound is demonstrated for only four nodes (9, 12 and 18) of the feeder with the addition of three MGs. In [39], the 5kW solar PV system installed with a pumped hydro system was made to operate in time series to evaluate the voltage performance as a function of generic load profile and output power generated. The same situation applies to [38]. In the present study, the EVs charging is isolated from contributing back into the grid through a unidirectional converter. This prevents the grid stress toward voltage collapse at peak load conditions to achieve conformity to voltage operating limits at all hours. Unlike the study in [40], the EVs are configured to directly drawn power from the main grid. The network operation can be thrown off equilibrium at peak load conditions. Although the vehicle to grid technology was in place to support the system at peak condition, however, connecting such a model with a more extensive network with high load demand will not give room for the vehicle to grid to operate sufficiently at emergency due to high load demand and comprehensive system.

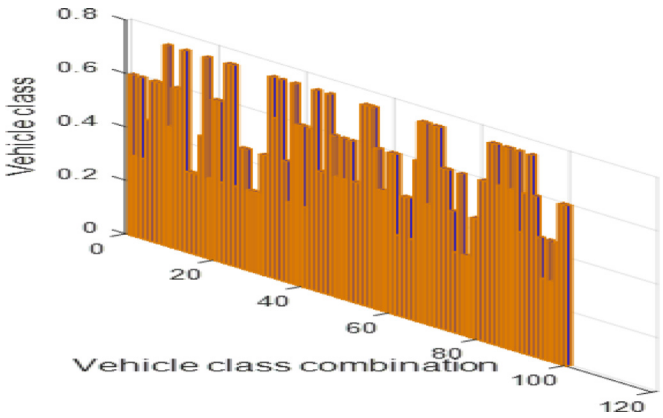

Fig. 24. The vehicle class distribution.

6. Conclusions

A hybrid solar PVSHP is modeled in EVs grid isolated MEG connected on the smart distribution network. A decentralized multi-agent system was applied for smart network voltage regulation through online regulation of network reactive power compensation. The complementary action of solar and small hydro generation is annexed into the grid via a load-following strategy incorporated a local means of control. The proposed model was tested and verified by implementing it on 1EEE 33 and IEEE 118 node feeders. The percentage voltage improvement in 33 bus system with the proposed technique is 48.5% using one microgrid integration. With two microgrid integration, the percentage improvement is 72.39%. The voltage profile within the statutory limit is achieved. This occurred at all nodes of the feeder at all

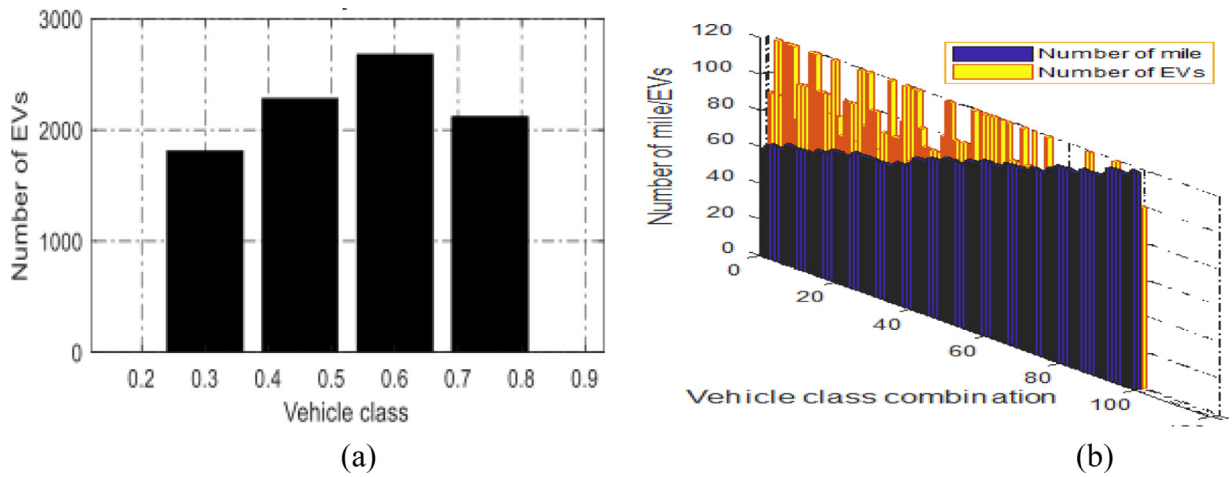

Fig. 23. (a) Cumulative number of EVs per vehicle class (b) The number of EVs and miles per day.

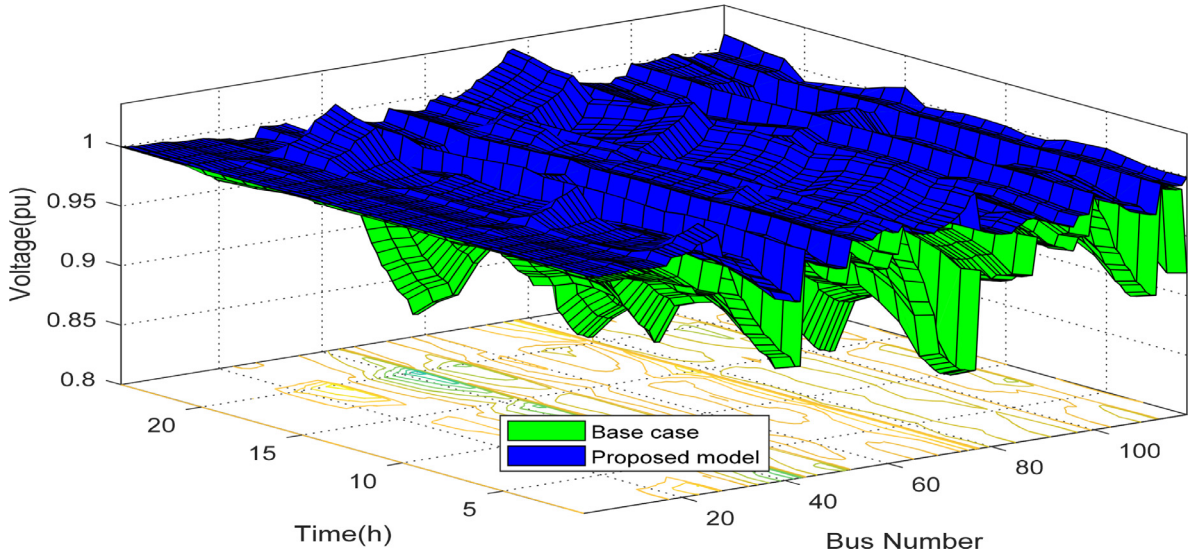

Fig. 25. Voltage profile for 118-bus system comparing base to the proposed model.

Table 4.
Voltage profile and power losses in IEEE 118 bus feeder.

Items	Without DG	With MG(Proposed model) One MG PVSHP/ESS @bus 2	Two MG	THREE MG PVSHP/ESS @bus 2&18	FOUR MG
Total losses(base)kW	32292.90	32292.90	32292.90	32292.90	32292.90
Total losses(kW)		23389.00	21446.00	19615.00	17575.00
Loss reduction (%)		27.57	33.59	39.25	45.50
Min voltage	0.8665 @bus 77, 20h	0.9356 @bus 43,20h	0.9457 @bus 43,20h	0.9520 @bus 43,20h	0.9685 @bus 43,20h
Max voltage	1.000 @bus 1&2,	1.035 @bus 27,19h	1.035 @bus 27,19h	1.035 @bus 27,19h	1.036 @bus 27,19h
Voltage imp (%)		24.03	28.08	37.06	40.50

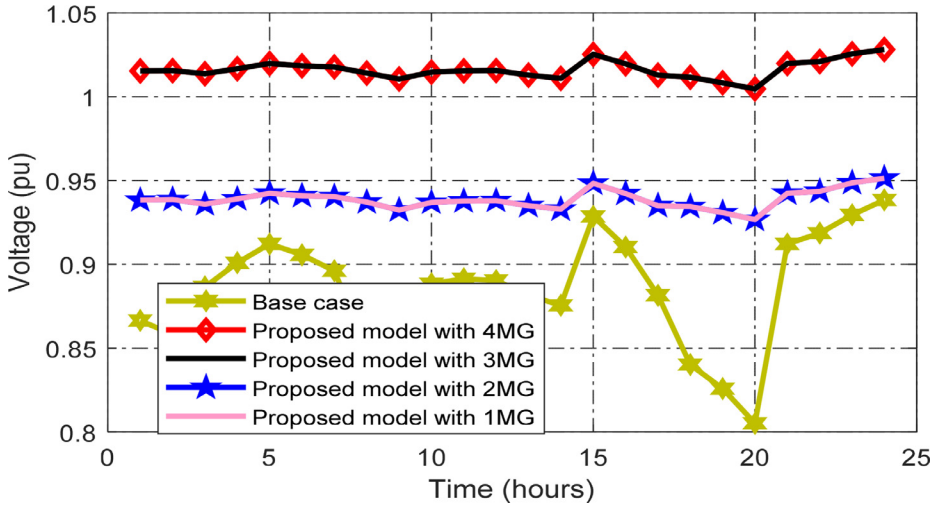

Fig. 26. Voltage profile at bus 77 for different microgrid integration level.

hours of the day. However, it took the integration of four microgrids to realize voltage within the bound in the 118 bus system. The grid isolated configuration of the EVs charging system guarantees the avoidance of network stress toward failure during the peak hours of the day and ensuring uninterruptable power supply while renewable synergized in the complementary injection of power.

CRediT author statement

Oladepo Olatunde: Conceptualization, Methodology, Software, Writing- Original draft preparation, Data curation, Visualization, Investigation, **Mohammad Yusri Hassan**: Supervision, Reviewing and Editing, **Md Pauzi Abdullah:** Supervision. **Hasimah Abdul Rahman:** Supervision.

Declaration of Competing Interest

The authors declare that they have no known competing financial interests or personal relationships that could have appeared to influence the work reported in this paper.

Table 5
Comparison of renewable system configuration and method with previous studies.

Configuration	Present study	Past Journals Paper 1 [38] (2013)	Paper 2 [1] (2018)	Paper 3 [39] (2018)
Renewable energy sources	PV & SHP	Wind & PV	PV & Biomass	PV & SHP
Metrological data simulation	Daily	Daily	Daily	Daily
PV module capacity(w)	200	165	none	none
Data modeling	Real-time	Real-time	Real-time	Forecasting
Standard IEEE bus system	33&118 bus	None	33 bus	None
Smart coordinating technique	Multi-agent system	None	Multi-agent system	Neural network
Excess power sink	Considered	None	None	None
Grid isolated EV charging	Considered	None	None	None
Local measurement control	MPPT& excitation control	None	None	None
Battery capacity sizing	Considered	None	None	None
Inverter sizing	Considered	None	None	None
Battery DOD	50%	None	None	None

References

[1] X. Wang, C. Wang, T. Xu, L. Guo, Optimal voltage regulation for distribution networks with multi-microgrids, Appl. Energy 210 (2018) 1027–1036, https://doi.org/10.1016/j.apenergy.2017.08.113.

[2] S.K. Khadem, M. Basu, M.F. Conlon, Capacity enhancement and flexible operation of unified power quality conditioner in smart and microgrid network, AIMS Energy 6 (2018) 49–69, https://doi.org/10.3934/energy.2018.1.49.

[3] R. Manimegalai, S. Visalakshi, S.L. Devi, Optimally locating microgrid for the minimization of losses, ICONSTEM 2017 – Proceedings of the Third IEEE International Conference on Science Technology and Engineering, Management, 2018, pp. 530–532, , https://doi.org/10.1109/ICONSTEM.2017.8261379 2018-Janua.

[4] A. Hatefi einaddin, A. Sadeghi Yazdankhah, R. Kazemzadeh, Power management in a utility connected micro-grid with multiple renewable energy sources, J. Oper. Autom. Power Eng. 5 (2017) 1–10, https://doi.org/10.22098/JOAPE.2017.543.

[5] I. Kim, Optimal distributed generation allocation for reactive power control, IET Gener. Transm. Distrib. 11 (2017) 1549–1556, https://doi.org/10.1049/iet-gtd.2016.1393.

[6] M. Gul, Y. Kotak, T. Muneer, Review on recent trend of solar photovoltaic technology, Energy Explor. Exploit. 34 (2016) 485–526, https://doi.org/10.1177/0144598716650552.

[7] Z. Salam, J. Ahmed, B.S. Merugu, The application of soft computing methods for MPPT of PV system: a technological and status review, Appl. Energy 107 (2013) 135–148, https://doi.org/10.1016/j.apenergy.2013.02.008.

[8] B. Pakkiraiah, G.D. Sukumar, Research survey on various MPPT performance issues to improve the solar PV system efficiency, J. Sol. Energy 2016 (2016) 1–20, https://doi.org/10.1155/2016/8012432.

[9] M.A. Elgendy, B. Zahawi, S. Member, D.J. Atkinson, Assessment of the incremental conductance maximum power point tracking algorithm, IEEE Trans. Sustain. Energy (2012) 1–10, https://doi.org/10.1109/TSTE.2012.2202698.

[10] W.C. Sheng, L. Hua, Y.Z. Long, W.Y. Bo, P.Y. Chang, X.H. Hua, Research on control strategies of small-hydro/PV hybrid power system, Proceedings of the First International Conference on Sustainable Power Generation, Supply, SUPERGEN '09. 1, 2009, pp. 1–5, , https://doi.org/10.1109/SUPERGEN.2009.5348119.

[11] W. Ali, M. Usama, H. Iqbal, A. Bashir, H. Farooq, Analyzing the impact of grid connected distributed micro-hydro generation under various fault conditions, Proceedings of the 2018 International Conference on Electric Engineering, 2018, pp. 1–6.

[12] W.M.M.G John Mbaka, Small hydro-power plants in Kenya: a review of status, challenges and future prospects, J. Renew. Energy Environ. 3 (2017) 20–26.

[13] I. Kougias, S. Szabó, F. Monforti-Ferrario, T. Huld, K. Bódis, A methodology for optimization of the complementarity between small-hydropower plants and solar PV systems, Renew. Energy 87 (2016) 1023–1030, https://doi.org/10.1016/j.renene.2015.09.073.

[14] A. Beluco, P. Kroeff de Souza, A. Krenzinger, A method to evaluate the effect of complementarity in time between hydro and solar energy on the performance of hybrid hydro PV generating plants, Renew. Energy 45 (2012) 24–30, https://doi.org/10.1016/j.renene.2012.01.096.

[15] C. Chardonnet, C. Czajkowski, R.R. Sanchez, Impact of electric vehicles on distribution network operation:real world case studies, (2016) 4–7.

[16] J. Hu, H. Morais, T. Sousa, M. Lind, Electric vehicle fleet management in smart grids: a review of services, optimization and control aspects, Renew. Sustain. Energy Rev. 56 (2016) 1207–1226, https://doi.org/10.1016/j.rser.2015.12.014.

[17] M. Sechilariu, B.C. Wang, F. Locment, A. Jouglet, DC microgrid power flow optimization by multi-layer supervision control. Design and experimental validation, Energy Convers. Manag. 82 (2014) 1–10, https://doi.org/10.1016/j.enconman.2014.03.010.

[18] A. Kuperman, U. Levy, J. Goren, A. Zafransky, A. Savernin, Battery charger for electric vehicle traction battery switch station, IEEE Trans. Ind. Electron. 60 (2013) 5391–5399, https://doi.org/10.1109/TIE.2012.2233695.

[19] A. Mohamed, V. Salehi, T. Ma, O. Mohammed, Real-time energy management algorithm for plug-in hybrid electric vehicle charging parks involving sustainable energy, IEEE Trans. Sustain. Energy 5 (2014) 577–586, https://doi.org/10.1109/TSTE.2013.2278544.

[20] M. Dreidy, H. Mokhlis, S. Mekhilef, Inertia response and frequency control techniques for renewable energy sources: a review, Renew. Sustain. Energy Rev. 69 (2017) 144–155, https://doi.org/10.1016/j.rser.2016.11.170.

[21] K.A. Alobeidli, M.H. Syed, M.S. El Moursi, H.H. Zeineldin, Novel coordinated voltage control for hybrid micro-grid with islanding capability, IEEE Trans. Smart Grid. 6 (2015) 1116–1127, https://doi.org/10.1109/TSG.2014.2372795.

[22] H. Lan, S. Wen, Q. Fu, D.C. Yu, L. Zhang, Modeling analysis and improvement of power loss in microgrid, Math. Probl. Eng. 2015 (2015), https://doi.org/10.1155/2015/493560.

[23] H. Ji, C. Wang, P. Li, A centralized-based method to determine the local voltage control strategies of distributed generator operation in active distribution networks, Appl. Energy 228 (2018) 2024–2036, https://doi.org/10.1016/j.apenergy.2018.07.065.

[24] C. Yammani, S. Maheswarapu, S. Matam, Optimal placement of multi DGs in distribution system with considering the DG bus available limits, Energy Power 2 (2012) 18–23, https://doi.org/10.5923/j.ep.20120201.03.

[25] A. Giwa, A. Alabi, A. Yusuf, T. Olukan, A comprehensive review on biomass and solar energy for sustainable energy generation in Nigeria, Renew. Sustain. Energy Rev. 69 (2017) 620–641, https://doi.org/10.1016/j.rser.2016.11.160.

[26] A.O. Adejumo, E.A. Suleiman, H.I. Okagbue, Exploration of solar radiation data from three geo-political zones in Nigeria, Data Br. 13 (2017) 60–68, https://doi.org/10.1016/j.dib.2017.05.017.

[27] G.K. Singh, Solar power generation by PV (photovoltaic) technology: a review, Energy 53 (2013) 1–13, https://doi.org/10.1016/j.energy.2013.02.057.

[28] J.O. Petinrin, M. Shaaban, Multiperiod coordination of local voltage controllers and energy storage for voltage regulation in distribution feeder-connected renewable energy sources, Iran, J. Sci. Technol. Trans. Electr. Eng. (2018), https://doi.org/10.1007/s40998-018-0092-2.

[29] N.D. Nordin, H. Abdul Rahman, A novel optimization method for designing stand alone photovoltaic system, Renew. Energy 89 (2016) 706–715, https://doi.org/10.1016/j.renene.2015.12.001.

[30] World Small Hydropower Development Report, United nations Industrial Development Organisation, Vienna and International Centre on Small Hydro Power, Hangzhou, 2016www.smallhydroworld.org (accessed 5 January 2020).

[31] Okinni Dam Small Hydro Power (SHP) Project, Min of Water Resources and Rural Development, Osun State Government Osogbo, Osun State, UNIDO Regional Centre for Small Hydro Power in Africa, Maitama, Abuja, 2008www.scribd.com (accessed 5 January 2020).

[32] T. Øyvang, G.J. Hegglid, B. Lie, Models of synchronous generators with excitation system, for transient power system studies, IFAC-PapersOnLine 51 (2018) 91–96, https://doi.org/10.1016/j.ifacol.2018.03.016.

[33] A. Mohamed, V. Salehi, T. Ma, O. Mohammed, Real-time energy management algorithm for plug-in hybrid electric vehicle charging parks involving sustainable energy, IEEE Trans. Sustain. Energy 5 (2014) 577–586, https://doi.org/10.1109/TSTE.2013.2278544.

[34] K. Yunus, H.Z. De La Parra, M. Reza, Distribution grid impact of plug-in electric vehicles charging at fast charging stations using stochastic charging model, Proceedings of the 2011 Fourteenth European Conference on Power Electronics and Application EPE 2011, 2011, pp. 1–11.

[35] M K.A., S A.A., A matlab based backward-forward sweep algorithm for radial distribution network power flow analysis, Int. J. Sci. Eng. Investig. 4 (2015) 89–96.

[36] P. D.P.R., V.C. V.R., T. G.M., Optimal renewable resources placement in distribution networks by combined power loss index and whale optimization algorithms, J. Electr. Syst. Inf. Technol. 5 (2018) 175–191, https://doi.org/10.1016/j.jesit.2017.05.006.

[37] D. Zhang, Z. Fu, L. Zhang, An improved TS algorithm for loss-minimum reconfiguration in large-scale distribution systems, Electr. Power Syst. Res. 77 (2007) 685–694, https://doi.org/10.1016/j.epsr.2006.06.005.

[38] M. Mikati, M. Santos, C. Armenta, Electric grid dependence on the configuration of a small-scale wind and solar power hybrid system, Renew. Energy 57 (2013) 587–593, https://doi.org/10.1016/j.renene.2013.02.018.

[39] P. Chaudhary, M. Rizwan, Energy management supporting high penetration of solar photovoltaic generation for smart grid using solar forecasts and pumped hydro storage system, Renew. Energy 118 (2018) 928–946, https://doi.org/10.1016/j.renene.2017.10.113.

[40] H. Fathabadi, Novel solar powered electric vehicle charging station with the capability of vehicle-to-grid, Sol. Energy. 142 (2017) 136–143, https://doi.org/10.1016/j.solener.2016.11.037.